A Novel Target Separation Algorithm Applied to The Two-Dimensional Spectrum for FMCW Automotive Radar Systems

Conference Paper · November 2017

CITATIONS
0

READS
25

6 authors, including:

Tai Fei
HELLA Group
14 PUBLICATIONS **22** CITATIONS
SEE PROFILE

Christopher Grimm
HELLA Group
5 PUBLICATIONS **1** CITATION
SEE PROFILE

Ernst Warsitz
HELLA Group
16 PUBLICATIONS **170** CITATIONS
SEE PROFILE

Reinhold Haeb-Umbach
Universität Paderborn
191 PUBLICATIONS **2,612** CITATIONS
SEE PROFILE

A Novel Target Separation Algorithm Applied to The Two-Dimensional Spectrum for FMCW Automotive Radar Systems

Tai Fei[(1)], Christopher Grimm[(1)], Ridha Farhoud[(1)], Tobias Breddermann[(1)], Ernst Warsitz[(1)], and Reinhold Häb-Umbach[(2)]

(1) Hella KGaA Hueck & Co., Beckumer Str. 130, 59552, Lippstadt Germany, {Tai.Fei, Christopher.Grimm. Tobias.Breddermann, Ernst.Warsitz}@Hella.com, (2) University of Paderborn, 33098 Paderborn, Germany, haeb@nt.uni-paderborn.de

***Abstract*—In this paper, we apply a high-resolution approach, i.e. the matrix pencil method (MPM), to the FMCW automotive radar system to separate the neighboring targets, which share similar parameters, i.e. range, relative speed and azimuth angle, and cause overlapping in the radar spectrum. In order to adapt the 1D model of MPM to the 2D range-velocity spectrum and simultaneously limit the computational cost, some preprocessing steps are proposed to construct a novel separation algorithm. Finally, this algorithm is evaluated in both simulation and real data, and the results indicate a promising performance.**

***Index Terms* — Matrix pencil method, target separation, FMCW radar, chirp sequence.**

I. Introduction

Due to the fast development of Gallium based material and the application of Complementary metal–oxide–semiconductor (CMOS) technology, the modern automotive radars can be constructed very compactly. Therefore, an increasing number of radar systems have been integrated in the vehicles for more complicated applications, such as environmental sensing. Compared to camera and lidar technologies, radar has its own unique advantages, i.e. high reliability in bad weather and lighting conditions; accurate and direct measurements of range, relative velocity, and angle of multiple targets; a high range coverage of up to 250 meters. Hence, radar is, today, an indispensable component in the advanced driver assistance systems (ADASs). However, thanks to the constraints on available bandwidth and hardware resources (e.g. storage limitation and computation power) of embedded systems, a commercial automotive radar is not able to achieve an arbitrarily fine resolution.

Conventional radar preprocessing, which nowadays is optimally supported by high speed hardware, consists pulse compression (range dimension), Doppler processing (velocity dimension), and angle of arrival determination (azimuth dimension) [1]. The utilization of linear chirp sequence modulation in current radar sensors, consequently, requires multidimensional Fourier transform as a preprocessing step. The following processing steps then take place in the multispectral space. Since the antenna aperture in automotive radar sensors is strictly bounded, the angular resolution is usually very rough. Thus, mostly target detection is conducted in the 2D subspace, i.e. range-velocity (RV) spectrum. Adjacently, target parameter estimations are carried out, which are the basis for more sophisticated postprocessing, e.g. target classification, target tracking, road heat map, etc. The classical target parameter estimation takes the assumption that there is no target overlapping in the RV spectrum, and this assumption can yet be violated in critical use cases because of the limited range, and velocity resolution.

In the literature, many high-resolution-algorithms have been mentioned without changing the measurement duration or the bandwidth to enhance the resolution, including Prony's method [2], autoregressive modelling [3], multiple signal classification (MUSIC) [4] by Schmidt, estimation of signal parameters via rotational invariance techniques (ESPRIT) [5] by Roy *et al.*, and matrix pencil method (MPM) [6] by Sarkar et al. In practice, the AR modelling needs the *a priori* knowledge about the process order, which is normally unknown. Moreover, both MUSIC and ESPRIT are based on the eigen-structure of the input covariance matrix. The estimation of covariance matrix is usually computationally intensive. In contrast, the MPM is a variation of the eigen-structure approach and takes advantage of the pencil matrix instead of the covariance matrix. Besides, the MUSIC and the AR-based spectral estimation algorithm yield out a spectrum function. The exact localization of potential frequency components demands a full spectral scan. A high resolution is dependent of the scan step width.

Recently in [7], the MPM has been firstly applied to the 1D (range dimension) FMCW radar spectrum in static scenarios. There is neither systematic performance comparison nor the elaborate adaption of MPM into the FMCW radar signal processing chain being presented by the authors. In this work, the MPM is modified and applied to the 2D RV spectrum as a high-resolution technique to distinguish the overlapping moving targets. In order to restrict the computational effort and maintain the real-time capacity, the conventional power detection based on local maximum in the RV spectrum is going to be retained for most of the targets. Hence, the input data of signal processing steps is the classical 2D RV spectrum. The modified MPM (MMPM) is employed only in the cases where the required resolution for target separation cannot be satisfied in the RV spectrum. In addition, the MMPM provide simultaneously also the phase information of overlapping targets, such that the angle of arrival can be determined. The remaining of this paper is going to be organized as followed. In section 2, the modelling of frequency estimation by using MPM is revisited. In section 3, the modification and adaption of MPM to the 2D RV spectrum is explained. Section 4 shows the performance in simulations and measurements, and finally in section 5 the conclusion is given.

978-1-5386-3169-0/17/$31.00 ©2017 IEEE

II. Modelling of Matrix Pencil Method

The energy point in power spectrum can be modelled as the superposition of multiple complex exponentials,

$$\begin{aligned} y(kT_s) &= x(kT_s) + n(kT_s) \\ &= \sum_{i=1}^{M} R_i z_i^k + n(kT_s)' \\ & k = 0, \dots, N-1, \end{aligned} \tag{1}$$

where $y(kT_s)$ and $n(kT_s)$ are the observed signal and system noise, respectively, and

$$z_i = e^{(-\alpha_i + j\omega_i)T_s}, i = 1, \dots, M, \tag{2}$$

in which T_s represents the sampling period and kT_s denotes the sampling time points, α_i and ω_i are the damping factor and angular frequency, respectively. Determining the parameters, i.e. the signal poles z_i, its residues R_i and the number of poles M, becomes a typical parametric estimation problem. The MPM offers a solution to find the best estimates, with which the observed signal $y(t)$ can be approximated with the least amount of errors.

First of all, the noise free case is considered to introduce the solution of MPM. The discrete signal model can be stored in the following matrix form:

$$\mathbf{Y} = \begin{pmatrix} x(0) & x(1) & \dots & x(L) \\ x(1) & x(2) & \dots & x(L+1) \\ \vdots & \vdots & \vdots & \vdots \\ x(N-L-1) & x(N-L) & \dots & x(N-1) \end{pmatrix}, \tag{3}$$

where the dimension of this matrix is $(N-L)\times(L+1)$. Then, two matrices $\mathbf{Y}_1$ and $\mathbf{Y}_2$ with dimensions $(N-L)\times L$ are defined as

$$\mathbf{Y}_1 = \begin{pmatrix} x(0) & x(1) & \dots & x(L-1) \\ x(1) & x(2) & \dots & x(L) \\ \vdots & \vdots & \vdots & \vdots \\ x(N-L-1) & x(N-L) & \dots & x(N-2) \end{pmatrix}, \tag{4}$$

and

$$\mathbf{Y}_2 = \begin{pmatrix} x(1) & x(2) & \dots & x(L) \\ x(2) & x(3) & \dots & x(L+1) \\ \vdots & \vdots & \vdots & \vdots \\ x(N-L) & x(N-L+1) & \dots & x(N-1) \end{pmatrix}. \tag{5}$$

According to [8], matrices $\mathbf{Y}_1$ and $\mathbf{Y}_2$ can be decomposed as:

$$\mathbf{Y}_2 = \mathbf{Z}_1 \cdot \mathbf{R} \cdot \mathbf{Z}_0 \cdot \mathbf{Z}_2, \tag{6}$$

$$\mathbf{Y}_1 = \mathbf{Z}_1 \cdot \mathbf{R} \cdot \mathbf{Z}_2, \tag{7}$$

where

$$\mathbf{Z}_1 = \begin{pmatrix} 1 & 1 & \dots & 1 \\ z_1 & z_2 & \dots & z_M \\ \vdots & \vdots & \vdots & \vdots \\ z_1^{N-L-1} & z_2^{N-L-1} & \dots & z_M^{N-L-1} \end{pmatrix}, \tag{8}$$

$$\mathbf{Z}_2 = \begin{pmatrix} 1 & z_1 & \dots & z_1^{L-1} \\ 1 & z_2 & \dots & z_2^{L-1} \\ \vdots & \vdots & \vdots & \vdots \\ 1 & z_M & \dots & z_M^{L-1} \end{pmatrix}, \tag{9}$$

$$\mathbf{Z}_0 = \begin{pmatrix} 1 & & & \\ & z_2 & & \\ & & z_3 & \\ & & & z_M \end{pmatrix}, \tag{10}$$

$$\boldsymbol{R} = \begin{pmatrix} R_1 & & & \\ & R_2 & & \\ & & \dots & \\ & & & R_M \end{pmatrix}. \tag{11}$$

Now consider to construct the matrix pencil function by using the above matrices:

$$\mathbf{Y}_2 - \lambda \mathbf{Y}_1 = \mathbf{Z}_1 \cdot \mathbf{R} \cdot (\mathbf{Z}_0 - \lambda \mathbf{I}_M) \cdot \mathbf{Z}_2, \tag{12}$$

in which $\mathbf{I}_M$ is a $M\times M$ identity matrix, and $\mathbf{R}$ and $\mathbf{Z}_0$ are full rank $M\times M$ diagonal matrices. It is assumed that $\{\lambda_i | \, i = 1, .., M\}$ are the eigenvalues of matrix pencil $\mathbf{Y}_2 - \lambda \mathbf{Y}_1$. It has also been proven in [9] that if pencil parameter L fulfills the condition $M \le L \le N - M$, $\mathrm{Rank}\{\mathbf{Y}_2 - \lambda \mathbf{Y}_1\} = M$ for $\lambda \notin \{\lambda_i | i = 1, \dots, M\}$. Hence, we let $M \le L \le N - M$. If $\lambda = z_i$, then $(\mathbf{Z}_0 - \lambda \mathbf{I}_M)_{i,i} = 0$, the i-th column of $\mathbf{Z}_1$ and i-th row of $\mathbf{Z}_2$ are removable. Then,

$$\mathrm{Rank}\{\mathbf{Y}_2 - \lambda \mathbf{Y}_1\} = M - 1, \tag{13}$$

where z_i is a rank reducing number of the matrix pencil $\mathbf{Y}_2 - \lambda \mathbf{Y}_1$. Moreover, the signal poles z_i are equal to the eigenvalue λ_i, since the rank of $\mathbf{Y}_2 - \lambda \mathbf{Y}_1$ decreases only at $\lambda = z_i$ and only by one. Thus, the problem of finding the signal poles z_i can be casted as generalized eigenvalue problem of matrix pencil z_i. With the help of Moore-Penrose pseudo inverse, the generalized eigenvalue problem can be degraded to the ordinary eigenvalue problem,

$$\begin{aligned} \boldsymbol{Y}_1^{+}(\boldsymbol{Y}_2 - \lambda \boldsymbol{Y}_1) &= \boldsymbol{Y}_1^{+}\boldsymbol{Y}_2 - \lambda (\boldsymbol{Y}_1^H \boldsymbol{Y}_1)^{-1} \boldsymbol{Y}_1^H \boldsymbol{Y}_1 \\ &= \boldsymbol{Y}_1^{+}\boldsymbol{Y}_2 - \lambda \boldsymbol{I}_M \end{aligned}, \tag{14}$$

where Moore-Penrose pseudo inverse $\mathbf{Y}_1^{+} = (\mathbf{Y}_1^H \mathbf{Y}_1)^{-1} \mathbf{Y}_1^H$, the superscript ^{H} denotes the conjugate transpose.

In noisy case, the signal storage matrix $\mathbf{Y}$ is given hereby as

$$\mathbf{Y} = \begin{pmatrix} y(0) & y(1) & \dots & y(L) \\ y(1) & y(2) & \dots & y(L+1) \\ \vdots & \vdots & \vdots & \vdots \\ y(N-L-1) & y(N-L) & \dots & y(N-1) \end{pmatrix}, \tag{15}$$

which should be denoised by selecting dominant signal through singular value decomposition,

$$\mathbf{Y} = \mathbf{U}\boldsymbol{\Sigma}\mathbf{V}^H, \tag{16}$$

where the rank of this noisy matrix in Eq. (16) $\mathrm{Rank}\{\mathbf{Y}\} \ge M$. Dependent of the separation demand and the actual noise level, M most dominant singular components are chosen,

$$\mathbf{Y}' = \mathbf{U}\boldsymbol{\Sigma}'\mathbf{V}'^H, \tag{17}$$

where $\boldsymbol{\Sigma}'$ is a diagonal matrix determined from $\boldsymbol{\Sigma}$ with M columns corresponding to the most dominant singular values. Like Eq. (4) and Eq. (5) in the noise free case, two other matrices can be rewritten as

$$\mathbf{Y}_2{}' = \mathbf{U}\boldsymbol{\Sigma}'\mathbf{V}_2{}'^H, \quad (18)$$

$$\mathbf{Y}_1{}' = \mathbf{U}\boldsymbol{\Sigma}'\mathbf{V}_1{}'^H, \quad (19)$$

in which $\mathbf{V}_2{}'$ obtained by discarding the first row of $\mathbf{V}'$, and $\mathbf{V}_1{}'$ is obtained by removing the last row of $\mathbf{V}'$. Then, the signal poles z_i can be figured out as the eigenvalues of matrix $(\mathbf{Y}_1')^+\mathbf{Y}_2{}'$, where the superscript $+$ indicates the Moore-Penrose pseudo inverse.

III. Target Separation In 2D Spectrum

The MPM introduced in the earlier section will be applied to the RV spectrum for the target separation purpose in this section, when target overlapping occurs in both dimensions. Since the spectra in the 1st and 2nd are independent, the target separation using MPM can theoretically take place in either range dimension or velocity dimension. In low ego speed cases, the stationary targets mostly have very similar even identical relative radical velocity. The target separation would be suggested in range dimension only. In other cases, the performances of the separations in range and velocity dimensions will be analyzed in Section 4.

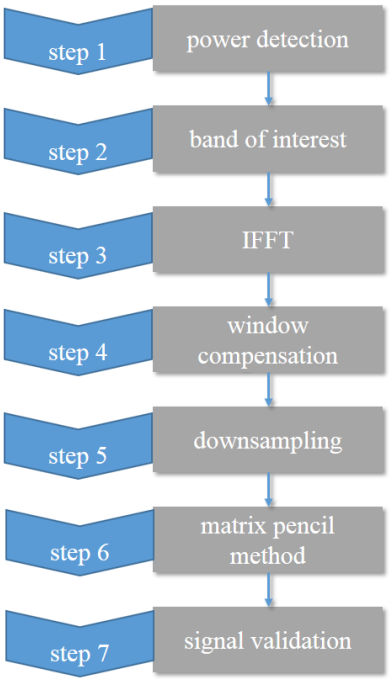

Figure 1 Modified MPM (MMPM) signal processing chain

As already stated in the introduction, MPM is only employed when necessary. The input data of this target separation problem is RV spectrum, and the choice of band of interest in spectrum for target separation is based on the local maximum search with power detection. Before applying the solution in section 2, the band of interest should be converted to time domain by inverse Fourier transform (IFFT), and the window function effect must also be compensated. Finally, the results given by the MPM solution should be verified. The complete the processing chain, which is named after modified MPM is summarized in the following figure,

A. Power Detection (Step 1)

Only those points in the RV spectrum, whose amplitudes are larger than a given threshold, are found from the RV spectrum. The threshold determination is normally CFAR oriented. The noise distribution can be estimated over several neighboring cycles. With assumption of the complex Gaussian distribution of the noise in Fourier spectrum, the noise amplitude square conforms to the gamma distribution. Given the false alarm rate β, the detection threshold $\mathcal{T}$ can be obtained as

$$\mathcal{T} = \mathcal{G}^{-1}(1-\beta), \quad (20)$$

where $\mathcal{G}^{-1}$ denotes the inverse gamma distribution function.

B. Band of Interest Selection (Step 2)

As already mentioned before, the high-resolution approach will not be universally applied to all the local maxima over the threshold $\mathcal{T}$. The selection of potential overlapping targets is a kind of the preselection, which should preferably guarantee a very low miss-recognition of overlapping targets at the cost of a relatively high false alarm. In the 2D RV spectrum, the BoI can be selected either in the range dimension or the velocity dimension.

This preselection can be performed by investigating the shape of the local maxima which are over $\mathcal{T}$. An intuitive approach is to examine the widths of the local maxima over the detection threshold in individual dimensions. If the width is larger than a certain threshold, it could be believed that target overlapping is probably happened here. Moreover, template matching based technique is a more sophisticated approach. Given a spectrum S_T of a monotone signal, the normalized cross-correlation between a detected local maximum and S_T indicates the potential of target overlapping. A cross-correlation close to 1 indicates that the target overlapping is almost impossible.

After the selection of potential overlapping targets, a certain frequency band of interest (BoI) around the detected local maximum is selected. Enough peak information should be guaranteed, so that the correct range or velocity (Doppler) frequency of the targets of interest can be extracted from the selected BoI. There are a certain number of points around a local maximum, which is significantly larger than zero, while the other points under the threshold $\mathcal{T}$ can be approximated as zero. This implies that most of the target information is included in those non-zero points. On the other side, the BoI cannot be set too wide because unwanted sidelobe from other signal spectral responses or noise could be included and distort the estimation of the desired targets. The BoI $S_{\mathrm{BoI}}(n)$ can be denoted as:

$$S_{\mathrm{BoI}}(n) = \begin{cases} S(n), & N_l \le n \le N_r \\ 0, & \text{others} \end{cases}, \quad (21)$$

$$\text{for } 0 \le n \le N' - 1$$

where $S(n)$ denotes the spectral function of either range dimension or velocity dimension in the 2D RV spectrum, N' is the number of sampling points in the frequency. It corresponds to the length of either range dimension or velocity dimension in RV spectrum. The BoI should be shifted into the low frequency region to decrease the

computational cost in time domain for the following processing,

$$S'_{\mathrm{BoI}}(n') = \begin{cases} S(n'+N_l), & 0 \le n \le N'-N_l \\ 0, & \text{others} \end{cases}, \quad \text{for } 0 \le n \le N'-1 \tag{22}$$

where N_l denotes the shifted frequencies in bin. The illustration of $S_{\mathrm{BoI}}(n)$ and $S'_{\mathrm{BoI}}(n')$ can be found in Fig. 2.

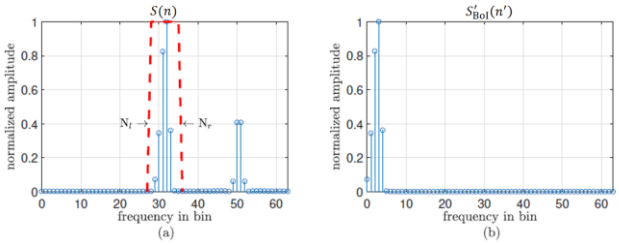

Figure 2(a) The BoI in the original frequency domain. (b) The BoI in the low frequency domain.

C. Inverse finite Fourier transform (Step 3)

The inverse finite Fourier transform (IFFT) converts the signal in BoI into time domain, where the model of MPM, cf. Eq. (1) and Eq. (2), is developed,

$$S'_{\mathrm{BoI}}(n') \xrightarrow{\mathcal{F}^{-1}} s_{\mathrm{BoI}}(\mathcal{V}), \mathcal{V} = 0, \dots, N'-1. \tag{23}$$

D. Window Compensation (Step 4)

In practice, a window function, e.g. Hamming window, is usually adopted to reduce the sidelobe of significant signal in

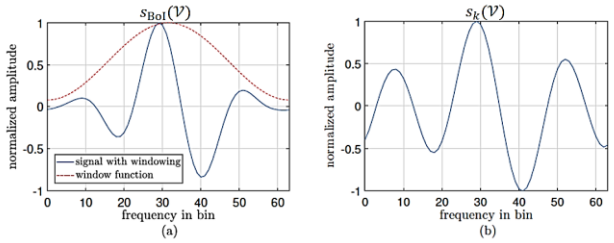

Figure 3 (a) Time signal before compensating windowing effect. (b) Time signal after compensating windowing.

the spectrum. Theoretically, we can also incorporate the window function in the modelling in Eq. (1). However, the solution becomes complicated. Since the window function is known, we can compensate its effect as follows,

$$s_k(\mathcal{V}) = \frac{s_{\mathrm{BoI}}(\mathcal{V})}{w(\mathcal{V})}, \mathcal{V} = 0, \dots, N'-1, \tag{24}$$

where $w(\mathcal{V})$ denotes the window function, and $s_{\mathrm{BoI}}(\mathcal{V})$ and $s_k(\mathcal{V})$ are shown in Fig. 3.

E. Downsampling (Step 5)

Since the BoI is selected in the previous step, the bandwidth is henceforth limited. This BoI is also shifted to low frequency region, and according to the Nyquist criterion, the number of sampling values in time domain can be reduced without losing the signal information by downsampling

$$s_d(\tilde{\mathcal{V}}) = s_k(D\tilde{\mathcal{V}} + n_p), \quad 0 \le \tilde{\mathcal{V}} \le N_s - 1, 0 \le n_p \le D-1, \tag{25}$$

and

$$N_s = \left\lfloor \frac{N'}{D} \right\rfloor, \tag{26}$$

where the integer value D denotes the downsampling rate, N_s is the number of points after downsampling, and n_p is an offset value. This downsampling also reduces the computational effort in MPM. Due to some small values at the edges of window functions (e.g. the Blackman and Hann window), the division operation in Eq. 26 can cause some numeric instability problem at the edge of windows. Therefore, the downsampling should omit these points, i.e. $n_p = 0$ and $n_p \neq D-1$.

F. Band of Interest Selection (Step 6)

So far, the spectrum signal $S(n)$ (either range dimension or velocity dimension) obtained in RV spectrum is processed and transformed into time domain, cf. $s_d(\tilde{\mathcal{V}})$, which corresponds to the signal model in Eq. (1), and the MPM provides the solution to determine the signal parameters, i.e. signal poles z_i, its residue R_i and the number of frequency components M. The angular frequency in the low frequency region can be extracted by

$$\omega_{d_i} = \frac{\phi(z_i)}{T_d}, i = 1, \dots, M \tag{27}$$

and the sampling period can be represented as:

$$T_d = D \cdot T_s \tag{28}$$

where T_s denotes the sampling period (In range dimension, it denotes the ADC converter sampling period, and in velocity dimension it is chirp to chirp interval duration.), $\phi(z_i)$ stands for the phase of the complex signal z_i. Subsequently, the angular frequency ω_{d_i} should be frequency-shifted back into original frequency region to obtain the correct range or Doppler frequency:

$$f_i = \frac{\omega_{d_i}}{2\pi} + N_l \cdot \Delta f, \tag{29}$$

where Δf means the frequency resolution in consideration. To this end, the possible number of signals M, the frequency f_i and its complex amplitude R_i are found. Moreover, the complex R_i contains the phase information of individual signal component in the overlapping. The above-mentioned processing can be repeated on another antenna. Using the difference between the two phases obtained in both antennas, the angle of arrival (AoA) of the overlapping targets can be found. It is also called monopulse AoA estimation method.

G. Signal Selection (Step 7)

In this step, several criteria are developed to further filter out the implausible signals obtained in previous step. Those

implausible signals could be caused by the environment noise

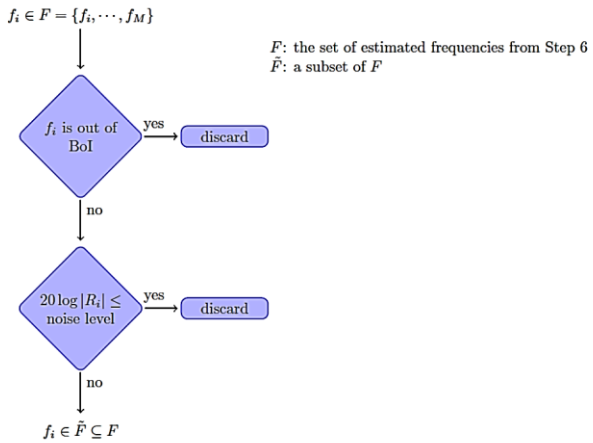

Figure 4 Flow chart of the signal selection

and sidelobes leaking from other signal spectral responses. As shown in Figure 4, those frequencies which are outside of the BoI should be discarded. What is more, those signals whose amplitudes are under the noise level should also be discarded.

IV. Evaluation with Simulation and Measurements

In this section, the performance of estimating range, relative velocity and AoA via MMPM in the framework of Hella 24 GHz radar system is analyzed using numerical simulation in Matlab and real measurement data. To avoid losing generality, the RV-spectrum is modified, such that the range axis in [m] and the relative velocity axis in [m/s] are normalized to the range and Doppler frequency in [bin], respectively. Target parameters including the range, velocity, AoA, and target amplitude are considered as variables. Environment parameters mainly refer to the noise. The numerical results using MATLAB are based on Monte-Carlo simulation. We define the mean absolute error (MAE) as figure of merit,

$$\mathrm{MAE} = \frac{1}{N_m}\sum_{i=1}^{N_m}|\varsigma - \hat{\varsigma}_i|, \tag{30}$$

where N_m is the running index of Monte-Carlo simulation, ς is the ground truth, and $\hat{\varsigma}_i$ is the estimates, i.e. range and velocity. The signal-to-noise ratio (SNR) of i-th signal is defined as

$$\mathrm{SNR}_i = 10\log_{10}\frac{|A_i|^2}{\mathrm{NL}}, \tag{31}$$

where A_i is the amplitude of i-th signal, and NL is the noise level, with which the false alarm rate is set to 2%.

A. Simulations

Two targets parameters are shown in Fig. 5, and they have similar ranges and relative velocities. The frequency difference in range and velocity dimensions are denoted as δf_r and δf_v, respectively, and they are set to $\delta f_r = 0.5$ bin and $\delta f_v = 0.5$ bin, cf. Fig. 5. The amplitude of the two targets are identical, i.e. $A_2 - A_1 = 0$. Because of noise effect and the fact that two targets have the same amplitudes, the observed peak in the RD-spectrum should stand either at 30 or 31 bin in the range frequency domain, and at 20 or 21 bin in the Doppler frequency domain. The SNRs of both targets vary from 0 to 70 dB. The Fig. 6 presents the MAEs of estimating the range and Doppler frequencies via MMPM. Starting from 30 dB, the MAEs of the separation in the range and velocity dimensions are smaller than 0.5 bin.

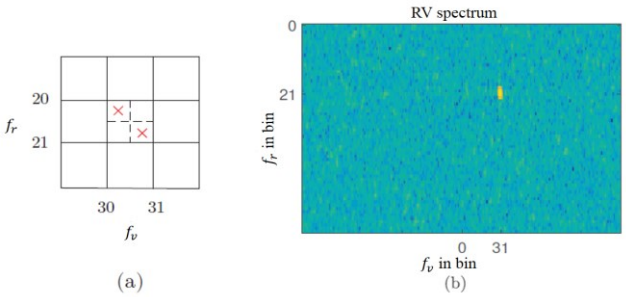

Figure 5 (a) Two targets overlap in one resolution bin. (b) The RD-spectrum of two overlapping targets.

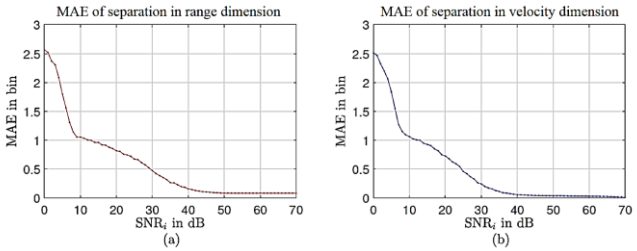

Figure 6 The MAEs of the estimated range and velocity frequencies of two overlapping targets. (a) range dimension separation, (b) velocity dimension separation.

Moreover, the separation ability in clutter scenario is studied. A guardrail is modeled close to the target, as shown in Fig. 7(a). Four Targets in four different scenarios are simulated, respectively. In case 1, target 1 locates on the left side of guardrail, and the remaining are on the left side. The guardrail will not completely cover target 1. Hence, target 1 can be seen by radar. In the RV spectrum in Fig. 7(b), the guardrail can be observed as clutter and will have affect the estimation of other moving targets.

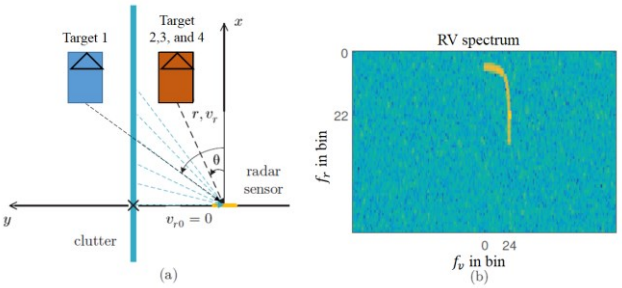

Figure 7(a) The sketch illustrates the desired target confused by clutter. (b) The target and the clutter overlapping in the RV spectrum.

The signal-to-clutter ratio (SCR) is defined as:

$$SCR = 10\,log_{10}\frac{|A|^2}{|C|^2}, \tag{32}$$

where A is the target amplitude and C denotes the average amplitude of clutter. In Fig. 8, the AoAs of four targets with different SCRs via the conventional local maximum

detection, and MMPM are compared. In the overlapping situation, local maximum detection recognizes only one target, and its parameter is disturbed by the other overlapping target. As shown in Fig. 8(a), Fig. 8(b) and Fig. 8(c), the estimated AoAs via the MMPM (green points) are more accurate than conventional local maximum detection (also called peak detection). In those three cases, the estimated AoAs via peak detection are always located between the clutter and the real target. Moreover, compared with the estimated AoAs of target 2 in Fig. 8(b), the estimated AoAs of target 3 in Fig. 8(c) via both methods get closer to the clutter, since the SCR is smaller in Fig. 8(c), namely -15 dB. Besides, as shown in Fig. 8(d), the predicted AoAs of target 4 can be precisely detected via both the peak detection algorithm and the MMPM, because the signal amplitude is much larger than the average clutter amplitude (SCR $=$ 15 dB).

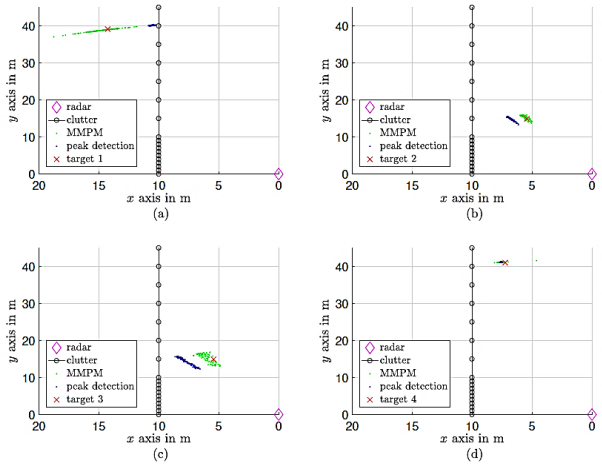

Figure 8 The estimated locations via the MMPM and the local maximum detection in the scenario that the target overlaps with a guardrail. (a) Target 1: $f_r = 21$ bin, $f_v = 24$ bin, $DoA = 20°$, $SCR = -15$ dB and $SNR = 30\,dB$. (b) Target 2: $f_r = 8$ bin, $f_v = 20$ bin, $DoA = 20°$, $SCR = -5$ dB and $SNR = 30\,dB$. (c) Target 3: $f_r = 8$ bin, $f_v = 20$ bin, $DoA = 20°$, $SCR = -15$ dB and $SNR = 30\,dB$. (d) Target 4: $f_r = 21$ bin, $f_v = 23$ bin, DoA $= 10°$, $SCR = 15\,dB$ and $SNR = 20\,dB$.

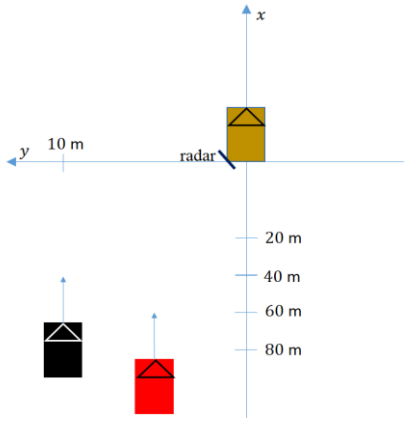

Figure 9 The test scenario illustration

Finally, the MMPM is applied to the real radar measurement, in which a test scenario in test field is recoded. In this scenario, two target vehicles are driving parallel heading to the radar sensor, cf. Fig. 9. The two target vehicles have similar distances to radar, and their velocities are almost identical. In Fig. 10, it can be found the MMPM can principally separate the trajectories of two targets, while the peak detection can only provide a mixture of the two trajectories.

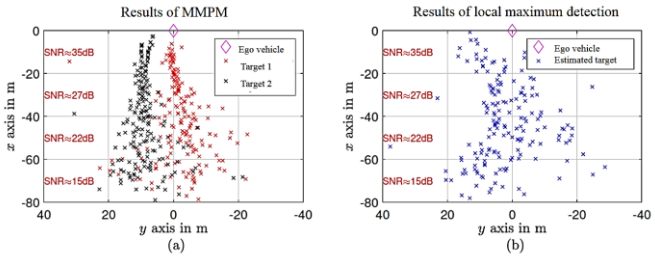

Figure 10 (a) the results of MMPM separation, (b) the results of conventional local maximum detection.

V. Conclusion

The application of MMPM to 2D RV radar spectrum provides a good performance in target separation. The separation performances in range dimension and velocity dimension are comparable. This method achieves a small MAE, when the SNR is greater than 25 dB. Moreover, MMPM makes it possible to estimate the AoA of overlapping targets via monopulse angle estimation approach.

References

[1] F. Engels, P. Heidenreich, and A. M. Zoubir, "Advances in Automotive Radar: A framework on computationally efficient high-resolution frequency estimation," *IEEE Signal Processing Magazine,* vol. 34, no. 2, pp. 36-46, Mar. 2017.

[2] R. Prony, "Essai exp´erimental et analytique sur les lois de la dilabilit´e des fluides ´elastiques, et sur celles de la force expansive de la vapeur de l'eau et de la vapeur de l'alkool, `a diff´erentes temp´eratures", *Paris J. I'Ecola Polytechnique*, 1, Calvier 2, pp. 24-76, 1795.

[3] F. S. Schlindwein, D. H. Evans, "Autoregressive spectral analysis as an alternative to fast Fourier transform analysis of Doppler ultrasound signals", 1992.

[4] Schmidt, R.O., "Multiple emitter location and signal parameter estimation", *IEEE Transactions on Antennas and Propagation*, vol 34, no. 3, pp. 276-280, March 1986.

[5] R. Roy and T. Kailath, "EPRIT–estimation of Signal parameters via rotational invariance techniques", *IEEE Transactions on Signal Processing*, vol 37, no. 7, pp. 984-995, July 1989.

[6] T. Sarkar, and O. Pereira, "Using the matrix pencil method to estimate the parameters of a sum of complex exponentials", *IEEE Antennas and Propagation Magazine*, vol. 37, no. 1, pp. 48-55, February 1995

[7] S. Olbrich and C. Waldschmidt: "New pre-estimation algorithm for FMCW radar systems using the matrix pencil method," *Proceedings of the 12th European Radar Conference*, pp- 177-180, 2015.

[8] T. Sarkar, and O. Pereira, "Using the matrix pencil method to estimate the parameters of a sum of complex exponentials," *IEEE Antennas and Propagation Magazine*, vol. 37, no. 1, pp. 48-55, February, 1995.

[9] Y. Hua, and T. Sarkar, "Matrix pencil method for estimating parameters of exponentially damped/undamped sinusoids in noise", *IEEE Transactions on Acoustics*, Speech and Signal Processing, vol 38, no. 5, pp. 814-824, May 1990.